

# NNLO corrections to event shapes in $e^+e^-$ annihilation

---

**A. Gehrmann–De Ridder**

*Institute for Theoretical Physics, ETH, CH-8093 Zürich, Switzerland*

*E-mail:* gehra@phys.ethz.ch

**T. Gehrmann**

*Institut für Theoretische Physik, Universität Zürich, Winterthurerstrasse 190,  
CH-8057 Zürich, Switzerland*

*E-mail:* thomas.gehrmann@physik.unizh.ch

**E.W.N. Glover**

*Institute of Particle Physics Phenomenology, Department of Physics,  
University of Durham, Durham, DH1 3LE, UK*

*E-mail:* e.w.n.glover@durham.ac.uk

**G. Heinrich**

*School of Physics, The University of Edinburgh, Edinburgh EH9 3JZ, UK*

*E-mail:* gheinric@ph.ed.ac.uk

**ABSTRACT:** We compute the next-to-next-to-leading order (NNLO) QCD corrections to the six most important event shape variables related to three-particle final states in electron-positron annihilation. The corrections are sizeable for all variables, however their magnitude is substantially different for different observables. We observe that the NNLO corrections yield a considerably better agreement between theory and experimental data both in shape and normalisation of the event shape distributions. The renormalisation scale dependence of the theoretical prediction is substantially reduced compared to the previously existing NLO results. Our results will allow a precise determination of the strong coupling constant from event shape data collected at LEP.

**KEYWORDS:** QCD, Jets, LEP HERA and SLC Physics, NLO and NNLO Computations.

---

## Contents

<b>1. Introduction</b>	<b>1</b>
<b>2. Event shape variables</b>	<b>2</b>
<b>3. Event shapes in perturbation theory</b>	<b>5</b>
<b>4. Calculation of NNLO corrections</b>	<b>7</b>
<b>5. NNLO distributions</b>	<b>9</b>
5.1 Thrust	10
5.2 Heavy jet mass	11
5.3 Jet broadenings	12
5.4 $C$ -parameter	13
5.5 $Y_3$	13
<b>6. Comparison with data</b>	<b>14</b>
6.1 Thrust	14
6.2 Heavy jet mass	15
6.3 Jet broadenings	17
6.4 $C$ -parameter	22
6.5 $Y_3$	24
<b>7. Conclusions and Outlook</b>	<b>26</b>

---

## 1. Introduction

For more than a decade experiments at LEP (CERN) and SLC (SLAC) gathered a wealth of high precision high energy hadronic data from electron-positron annihilation at a range of centre-of-mass energies [1–5]. This data provides one of the cleanest ways of probing our quantitative understanding of QCD. This is particularly so because the strong interactions occur only in the final state and are not entangled with the parton density functions associated with beams of hadrons. As the understanding of the strong interaction, and the capability of making more precise theoretical predictions, develops, more and more stringent comparisons of theory and experiment are possible, leading to improved measurements of fundamental quantities such as the strong coupling constant [6].

In addition to measuring multi-jet production rates, more specific information about the topology of the events can be extracted. To this end, many variables have been introduced which characterise the hadronic structure of an event. For example, we can ask

how planar or how collimated an event is. In general, a variable is described as  $n$  jet-like if it vanishes for a final state configuration of  $(n - 1)$  hadrons<sup>1</sup>. With the precision data from LEP and SLC, experimental distributions for such event shape variables have been extensively studied and have been compared with theoretical calculations based on next-to-leading order (NLO) parton-level event generator programs [7–9], improved by resumming kinematically-dominant leading and next-to-leading logarithms (NLO+NLL) [10, 11] and by the inclusion of non-perturbative models of power-suppressed hadronisation effects [12].

Comparing the different sources of error in the extraction of  $\alpha_s$  from hadronic data, one finds that the purely experimental error is negligible compared to the theoretical uncertainty. There are two sources of theoretical uncertainty: the theoretical description of the parton-to-hadron transition (hadronisation uncertainty) and the uncertainty stemming from the truncation of the perturbative series at a certain order, as estimated by scale variations (perturbative or scale uncertainty). Although the precise size of the hadronisation uncertainty is debatable and perhaps often underestimated, it is conventional to consider the scale uncertainty as the dominant source of theoretical error on the precise determination of  $\alpha_s$  from three-jet observables.

For the bulk of the paper we are concerned with the next-to-next-to-leading order (NNLO) perturbative corrections to three jet-like shape variables. To be precise, we present the NNLO coefficients for the differential distributions of thrust, the wide and total jet broadening, heavy hemisphere mass,  $C$  parameter and the jet transition variable  $Y_3$  for the Durham jet algorithm. These results are obtained using a numerical implementation of the two-loop  $\gamma^* \rightarrow 3$  parton [13], the one-loop  $\gamma^* \rightarrow 4$  partons [14] and the tree-level  $\gamma^* \rightarrow 5$  parton matrix elements [15]. Each of the contributions becomes singular when one or more partons are soft and/or collinear. In previous work, we have developed an antenna subtraction method [16] for isolating singularities and ensuring that the final result is infrared finite [17]. The resulting numerical program, **EERAD3**, yields the full kinematical information on the partonic final state and can be applied to generic infrared safe three-jet observables.

In section 2, we provide definitions of the relevant three-jet shape variables while section 3 reviews the structure of the perturbative predictions. Section 4 gives a brief description of the NNLO calculation and its implementation in the multi-purpose parton level Monte Carlo program **EERAD3**. Results for the event shape distributions are reported in sections 5 and 6, together with an estimate of the remaining perturbative uncertainty due to variations of the renormalisation scale. The parton level predictions are also compared with hadron-level experimental data. Finally, our results are summarised in section 7.

## 2. Event shape variables

In order to characterise hadronic final states in electron-positron annihilation, a variety of event shape variables have been proposed in the literature, for a review see e.g. [18].

---

<sup>1</sup>It should be noted that sometimes in the literature, especially in works on resummation, event shapes requiring three particles are called two-jet event shapes, while those requiring four particles are called three-jet event shapes.

These variables can be categorised into two classes, according to the minimal number of final-state particles required for them to be non-vanishing: the most common variables require three particles (and are thus closely related to three-jet final states), while several other variables were constructed such that they require at least four particles (related to four-jet final states).

Among the event shapes requiring three-particle final states, six variables were studied in great detail: the thrust  $T$  [19], the normalised heavy jet mass  $M_H^2/s$  [20], the wide and total jet broadenings  $B_W$  and  $B_T$  [21], the  $C$ -parameter [22] and the transition from three-jet to two-jet final states in the Durham jet algorithm  $Y_3$  [23].

(a) Thrust,  $T$  [19]

The thrust variable for a hadronic final state in  $e^+e^-$  annihilation is defined as [19]

$$T = \max_{\vec{n}} \left( \frac{\sum_i |\vec{p}_i \cdot \vec{n}|}{\sum_i |\vec{p}_i|} \right), \quad (2.1)$$

where  $\vec{p}_i$  denotes the three-momentum of particle  $i$ , with the sum running over all particles. The unit vector  $\vec{n}$  is varied to find the thrust direction  $\vec{n}_T$  which maximises the expression in parentheses.

The maximum value of thrust,  $T \rightarrow 1$ , is obtained in the limit where there are only two particles in the event. For a three-particle event the minimum value of thrust is  $T = 2/3$ .

(b) Heavy hemisphere mass,  $M_H^2/s$  [20]

In the original definition [20] one divides the event into two hemispheres. In each hemisphere,  $H_i$ , one also computes the hemisphere invariant mass as:

$$M_i^2/s = \frac{1}{E_{\text{vis}}^2} \left( \sum_{k \in H_i} p_k \right)^2, \quad (2.2)$$

where  $E_{\text{vis}}$  is the total energy visible in the event. In the original definition, the hemisphere is chosen such that  $M_1^2 + M_2^2$  is minimised. We follow the more customary definition whereby the hemispheres are separated by the plane orthogonal to the thrust axis.

The larger of the two hemisphere invariant masses yields the heavy jet mass:

$$\rho \equiv M_H^2/s = \max(M_1^2/s, M_2^2/s). \quad (2.3)$$

In the two-particle limit  $\rho \rightarrow 0$ , while for a three-particle event  $\rho \leq 1/3$ .

The associated light hemisphere mass,

$$M_L^2/s = \min(M_1^2/s, M_2^2/s) \quad (2.4)$$

is an example of a four-jet observable and vanishes in the three-particle limit.

At lowest order, the heavy jet mass and the  $(1 - T)$  distribution are identical. However, this degeneracy is lifted at next-to-leading order.

(c) Jet Broadening,  $B_W$  and  $B_T$  [21]

Taking a plane perpendicular to  $\vec{n}_T$  through the coordinate origin, one defines two event hemispheres  $H_{1,2}$ . In each of them, one determines the hemisphere broadening:

$$B_i = \frac{\sum_{k \in H_i} |\vec{p}_k \times \vec{n}_T|}{2 \sum_k |\vec{p}_k|} . \quad (2.5)$$

The wide and total jet broadening are then defined as

$$B_W = \max(B_1, B_2) , \quad (2.6)$$

$$B_T = B_1 + B_2 . \quad (2.7)$$

In the two-particle limit  $B_W \rightarrow 0$  and  $B_T \rightarrow 0$ . The maximum broadening for a three-particle event is  $B_T = B_W = 1/(2\sqrt{3})$ .

The narrow jet broadening,

$$B_N = \min(B_1, B_2) , \quad (2.8)$$

is another four-jet observable and vanishes when only three particles are in the event.

(d) The  $C$  parameter, [22]

The linearised momentum tensor

$$\Theta^{\alpha\beta} = \frac{1}{\sum_k |\vec{p}_k|} \sum_k \frac{p_k^\alpha p_k^\beta}{|\vec{p}_k|} , \quad (\alpha, \beta = 1, 2, 3) , \quad (2.9)$$

has three eigenvalues  $\lambda_i$ , which are used to construct the  $C$ -parameter:

$$C = 3 (\lambda_1 \lambda_2 + \lambda_2 \lambda_3 + \lambda_3 \lambda_1) . \quad (2.10)$$

This definition is equivalent to

$$C = 3 (\Theta^{11}\Theta^{22} + \Theta^{22}\Theta^{33} + \Theta^{33}\Theta^{11} - \Theta^{12}\Theta^{12} - \Theta^{23}\Theta^{23} - \Theta^{31}\Theta^{31}) . \quad (2.11)$$

The related four-jet observable is the  $D$ -parameter,

$$D = 27 \lambda_1 \lambda_2 \lambda_3 . \quad (2.12)$$

(e) The jet transition variable,  $Y_3$  [23]

The jet transition variable  $Y_3$  is defined as the value of the jet resolution parameter  $y_{\text{cut}}$  for which an event changes from a three-jet to a two-jet configuration with some jet defining scheme.

Here, we focus on the Durham jet algorithm which clusters particles into jets by computing the measurement variable

$$y_{ij,D} = \frac{2 \min(E_i^2, E_j^2)(1 - \cos \theta_{ij})}{E_{\text{vis}}^2} \quad (2.13)$$

for each pair  $(i, j)$  of particles. The pair with the lowest  $y_{ij,D}$  is replaced by a pseudoparticle whose four-momentum is given by the sum of the four-momenta of particles  $i$  and  $j$  ('E' recombination scheme). This procedure is repeated as long as pairs with invariant mass below the predefined resolution parameter  $y_{ij,D} < y_{\text{cut}}$  are found. Once the clustering is terminated, the remaining (pseudo-)particles are the jets.

### 3. Event shapes in perturbation theory

The perturbative expansion for the distribution of a generic observable  $y$  up to NNLO at centre-of-mass energy  $\sqrt{s}$  for renormalisation scale  $\mu^2 = s$  and  $\alpha_s \equiv \alpha_s(\sqrt{s})$  is given by

$$\frac{1}{\sigma_{\text{had}}} \frac{d\sigma}{dy} = \left(\frac{\alpha_s}{2\pi}\right) \frac{d\bar{A}}{dy} + \left(\frac{\alpha_s}{2\pi}\right)^2 \frac{d\bar{B}}{dy} + \left(\frac{\alpha_s}{2\pi}\right)^3 \frac{d\bar{C}}{dy} + \mathcal{O}(\alpha_s^4). \quad (3.1)$$

Here the event shape distribution is normalised to the total hadronic cross section  $\sigma_{\text{had}}$ . With the assumption of massless quarks, then at NNLO we have,

$$\sigma_{\text{had}} = \sigma_0 \left( 1 + \frac{3}{2} C_F \left( \frac{\alpha_s}{2\pi} \right) + K_2 \left( \frac{\alpha_s}{2\pi} \right)^2 + \mathcal{O}(\alpha_s^3) \right), \quad (3.2)$$

where the Born cross section for  $e^+e^- \rightarrow q\bar{q}$  is

$$\sigma_0 = \frac{4\pi\alpha}{3s} N e_q^2. \quad (3.3)$$

The constant  $K_2$  is given by,

$$K_2 = \frac{1}{4} \left[ -\frac{3}{2} C_F^2 + C_F C_A \left( \frac{123}{2} - 44\zeta_3 \right) + C_F T_R N_F (-22 + 16\zeta_3) \right], \quad (3.4)$$

where the QCD colour factors are

$$C_A = N, \quad C_F = \frac{N^2 - 1}{2N}, \quad T_R = \frac{1}{2} \quad (3.5)$$

for  $N = 3$  colours and  $N_F$  light quark flavours.

In practice, we compute the perturbative coefficients  $A$ ,  $B$  and  $C$ , which are all normalised to  $\sigma_0$ :

$$\frac{1}{\sigma_0} \frac{d\sigma}{dy} = \left(\frac{\alpha_s}{2\pi}\right) \frac{dA}{dy} + \left(\frac{\alpha_s}{2\pi}\right)^2 \frac{dB}{dy} + \left(\frac{\alpha_s}{2\pi}\right)^3 \frac{dC}{dy} + \mathcal{O}(\alpha_s^4). \quad (3.6)$$

However,  $A$ ,  $B$  and  $C$  are straightforwardly related to  $\bar{A}$ ,  $\bar{B}$  and  $\bar{C}$ ,

$$\begin{aligned}\bar{A} &= A, \\ \bar{B} &= B - \frac{3}{2}C_F A, \\ \bar{C} &= C - \frac{3}{2}C_F B + \left(\frac{9}{4}C_F^2 - K_2\right) A.\end{aligned}\tag{3.7}$$

These coefficients are computed at a renormalisation scale fixed to the centre-of-mass energy, and depend therefore only on the value of the observable  $y$ . They explicitly include only QCD corrections with non-singlet quark couplings and are therefore independent of electroweak couplings. At  $\mathcal{O}(\alpha_s^2)$ , these amount to the full corrections, while the  $\mathcal{O}(\alpha_s^3)$  corrections also receive a pure-singlet contribution. This pure-singlet contribution arises from the interference of diagrams where the external gauge boson couples to different quark lines. In four-jet observables at  $\mathcal{O}(\alpha_s^3)$ , these singlet contributions were found to be extremely small [24]. Also, the pure-singlet contribution from three-gluon final states to three-jet observables was found to be negligible [25]. This small correction to NNLO is denoted by  $\delta_C$ :

$$\left.\frac{1}{\sigma_0} \frac{d\sigma}{dy}\right|_{\text{NNLO, pure singlet}} = \left(\frac{\alpha_s}{2\pi}\right)^3 \frac{d\delta_C}{dy}(s, M_Z, \alpha, \sin^2 \Theta_W, c_q)\tag{3.8}$$

where  $c_q$  denotes the set of all electroweak vector and axial-vector quark couplings.

First-order electroweak corrections to event shape observables could be of a magnitude comparable to the NNLO QCD corrections. Like the pure-singlet NNLO contributions, these do also not factorise onto  $\sigma_0$ . The first-order electroweak corrections affect the distribution itself and the normalisation  $\sigma_{\text{had}}$ . Collectively, they give a contribution of the form,

$$\left.\frac{1}{\sigma_{\text{had}}} \frac{d\sigma}{dy}\right|_{\text{electroweak, } \mathcal{O}(\alpha\alpha_s)} = \left(\frac{\alpha}{2\pi}\right) \left(\frac{\alpha_s}{2\pi}\right) \frac{d\delta_{EW}}{dy}(s, M_Z, \alpha, \sin^2 \Theta_W, c_q).\tag{3.9}$$

These corrections are not complete at present [26], and clearly deserve further study.

In summary, the expression for event shape distributions accurate to NNLO in QCD and NLO in the electroweak theory reads:

$$\begin{aligned}\frac{1}{\sigma_{\text{had}}} \frac{d\sigma}{dy} &= \left(\frac{\alpha_s}{2\pi}\right) \frac{d\bar{A}}{dy} + \left(\frac{\alpha_s}{2\pi}\right)^2 \frac{d\bar{B}}{dy} + \left(\frac{\alpha_s}{2\pi}\right)^3 \frac{d\bar{C}}{dy} \\ &\quad + \left(\frac{\alpha_s}{2\pi}\right)^3 \frac{d\delta_C}{dy}(s, M_Z, \alpha, \sin^2 \Theta_W, c_q) \\ &\quad + \left(\frac{\alpha}{2\pi}\right) \left(\frac{\alpha_s}{2\pi}\right) \frac{d\delta_{EW}}{dy}(s, M_Z, M_H, \alpha, \sin^2 \Theta_W, c_q).\end{aligned}\tag{3.10}$$

In the following, we will focus on the QCD non-singlet expression (3.1), since  $\delta_C$  can be safely neglected, and the computation of  $\delta_{EW}$  needs further work.

The QCD coupling constant evolves according to the renormalisation group equation, which is to NNLO:

$$\mu^2 \frac{d\alpha_s(\mu)}{d\mu^2} = -\alpha_s(\mu) \left[ \beta_0 \left(\frac{\alpha_s(\mu)}{2\pi}\right) + \beta_1 \left(\frac{\alpha_s(\mu)}{2\pi}\right)^2 + \beta_2 \left(\frac{\alpha_s(\mu)}{2\pi}\right)^3 + \mathcal{O}(\alpha_s^4) \right]\tag{3.11}$$

with the  $\overline{\text{MS}}$ -scheme coefficients

$$\begin{aligned}\beta_0 &= \frac{11C_A - 4T_R N_F}{6}, \\ \beta_1 &= \frac{17C_A^2 - 10C_A T_R N_F - 6C_F T_R N_F}{6}, \\ \beta_2 &= \frac{1}{432}(2857C_A^3 + 108C_F^2 T_R N_F - 1230C_F C_A T_R N_F - 2830C_A^2 T_R N_F \\ &\quad + 264C_F T_R^2 N_F^2 + 316C_A T_R^2 N_F^2). \end{aligned} \quad (3.12)$$

Equation (3.11) is solved by introducing  $\Lambda$  as integration constant with  $L = \log(\mu^2/\Lambda^2)$ , yielding the running coupling constant:

$$\alpha_s(\mu) = \frac{2\pi}{\beta_0 L} \left( 1 - \frac{\beta_1}{\beta_0^2} \frac{\log L}{L} + \frac{1}{\beta_0^2 L^2} \left( \frac{\beta_1^2}{\beta_0^2} (\log^2 L - \log L - 1) + \frac{\beta_2}{\beta_0} \right) \right). \quad (3.13)$$

In terms of the running coupling  $\alpha_s(\mu)$ , the NNLO (non-singlet) expression for event shape distributions becomes

$$\begin{aligned} \frac{1}{\sigma_{\text{had}}} \frac{d\sigma}{dy}(s, \mu^2, y) &= \left( \frac{\alpha_s(\mu)}{2\pi} \right) \frac{d\bar{A}}{dy} + \left( \frac{\alpha_s(\mu)}{2\pi} \right)^2 \left( \frac{d\bar{B}}{dy} + \frac{d\bar{A}}{dy} \beta_0 \log \frac{\mu^2}{s} \right) \\ &\quad + \left( \frac{\alpha_s(\mu)}{2\pi} \right)^3 \left( \frac{d\bar{C}}{dy} + 2 \frac{d\bar{B}}{dy} \beta_0 \log \frac{\mu^2}{s} + \frac{d\bar{A}}{dy} \left( \beta_0^2 \log^2 \frac{\mu^2}{s} + \beta_1 \log \frac{\mu^2}{s} \right) \right) \\ &\quad + \mathcal{O}(\alpha_s^4). \end{aligned} \quad (3.14)$$

#### 4. Calculation of NNLO corrections

Three-jet production at tree-level is induced by the decay of a virtual photon (or other neutral gauge boson) into a quark-antiquark-gluon final state. At higher orders, this process receives corrections from extra real or virtual particles. The individual partonic channels that contribute through to NNLO are shown in Table 1. All of the tree-level and loop amplitudes associated with these channels are known in the literature [13–15, 27].

For a given partonic final state, the event shape observable  $y$  is computed according to the same definition as in the experiment, which is applied to partons instead of hadrons. At leading order, all three final state partons must be well separated from each other, such that  $y$  differs from the trivial two-parton limit. At NLO, up to four partons can be present in the final state, two of which can be clustered together, whereas at NNLO, the final state can consist of up to five partons, and as many as three partons can be clustered together. The more partons in the final state, the better one expects the matching between theory and experiment to be [28].

The two-loop  $\gamma^* \rightarrow q\bar{q}g$  matrix elements were derived in [13] by reducing all relevant Feynman integrals to a small set of master integrals using integration-by-parts [29] and Lorentz invariance [30] identities, solved with the Laporta algorithm [31]. The master integrals [32] were computed from their differential equations [30] and expressed analytically in terms of one- and two-dimensional harmonic polylogarithms [33].



---

LO	$\gamma^* \rightarrow q \bar{q} g$	tree level
NLO	$\gamma^* \rightarrow q \bar{q} g$	one loop
	$\gamma^* \rightarrow q \bar{q} g g$	tree level
	$\gamma^* \rightarrow q \bar{q} q \bar{q}$	tree level
NNLO	$\gamma^* \rightarrow q \bar{q} g$	two loop
	$\gamma^* \rightarrow q \bar{q} g g$	one loop
	$\gamma^* \rightarrow q \bar{q} q \bar{q}$	one loop
	$\gamma^* \rightarrow q \bar{q} q \bar{q} g$	tree level
	$\gamma^* \rightarrow q \bar{q} g g g$	tree level

---

**Table 1:** Non-singlet partonic contributions to three-jet event shape observables in perturbative QCD.

The one-loop four-parton matrix elements relevant here [14] were originally derived in the context of NLO corrections to four-jet production and related event shapes [34, 35]. One of these four-jet parton-level event generator programs [35] is the starting point for our calculation, since it already contains all relevant four-parton and five-parton matrix elements.

The four-parton and five-parton contributions to three-jet-like final states at NNLO contain infrared real radiation singularities, which have to be extracted and combined with the infrared singularities [36] present in the virtual three-parton and four-parton contributions to yield a finite result. In our case, this is accomplished by introducing subtraction functions, which account for the infrared real radiation singularities, and are sufficiently simple to be integrated analytically. Schematically, this subtraction reads:

$$\begin{aligned}
d\sigma_{NNLO} = & \int_{d\Phi_5} (d\sigma_{NNLO}^R - d\sigma_{NNLO}^S) \\
& + \int_{d\Phi_4} (d\sigma_{NNLO}^{V,1} - d\sigma_{NNLO}^{VS,1}) \\
& + \int_{d\Phi_5} d\sigma_{NNLO}^S + \int_{d\Phi_4} d\sigma_{NNLO}^{VS,1} + \int_{d\Phi_3} d\sigma_{NNLO}^{V,2} ,
\end{aligned}$$

where  $d\sigma_{NNLO}^S$  denotes the real radiation subtraction term coinciding with the five-parton tree level cross section  $d\sigma_{NNLO}^R$  in all singular limits [37]. Likewise,  $d\sigma_{NNLO}^{VS,1}$  is the one-loop virtual subtraction term coinciding with the one-loop four-parton cross section  $d\sigma_{NNLO}^{V,1}$  in all singular limits [38]. Finally, the two-loop correction to the three-parton cross section is denoted by  $d\sigma_{NNLO}^{V,2}$ . With these, each line in the above equation is individually infrared finite, and can be integrated numerically.

Systematic methods to derive and integrate subtraction terms were available in the literature only to NLO [39, 40]. Physical results for the special case of NNLO Higgs production have been achieved in [41]. In the context of this project, we fully developed an

NNLO subtraction formalism [16, 17, 42], based on the antenna subtraction method originally proposed at NLO [35, 40]. The basic idea of the antenna subtraction approach is to construct the subtraction terms from antenna functions. Each antenna function encapsulates all singular limits due to the emission of one or two unresolved partons between two colour-connected hard partons. This construction exploits the universal factorisation of phase space and squared matrix elements in all unresolved limits. The individual antenna functions are obtained by normalising three-parton and four-parton tree-level matrix elements and three-parton one-loop matrix elements to the corresponding two-parton tree-level matrix elements. Three different types of antenna functions are required, corresponding to the different pairs of hard partons forming the antenna: quark-antiquark, quark-gluon and gluon-gluon antenna functions. All these can be derived systematically from matrix elements [42] for physical processes.

The factorisation of the final state phase space into antenna phase space and hard phase space requires a mapping of the antenna momenta onto reduced hard momenta. We use the mapping derived in [43] for the three-parton and four-parton antenna functions. To extract the infrared poles of the subtraction terms, the antenna functions must be integrated analytically over the appropriate antenna phase spaces, which is done by reduction [44] to known phase space master integrals [45].

We tested the proper implementation of the subtraction by generating trajectories of phase space points approaching a given single or double unresolved limit. Along these trajectories, we observe that the antenna subtraction terms converge towards the physical matrix elements, and that the cancellations among individual contributions to the subtraction terms take place as expected. Moreover, we checked the correctness of the subtraction by introducing a lower cut (slicing parameter) on the phase space variables, and observing that our results are independent of this cut (provided it is chosen small enough). This behaviour indicates that the subtraction terms ensure that the contribution of potentially singular regions of the final state phase space does not contribute to the numerical integrals, but is accounted for analytically. A detailed description of the calculation can be found in [17].

The resulting numerical program, **EERAD3**, yields the full kinematical information on a given multi-parton final state. It can thus be used to compute any infrared-safe observable related to three-particle final states at  $\mathcal{O}(\alpha_s^3)$  in  $e^+e^-$ -annihilation.

## 5. NNLO distributions

In this section, we discuss the size and shape of the LO, NLO and NNLO coefficients of the perturbative expansion of the various event shape observables defined in Eq. (3.6). For convenience, we weight the distribution by the observable.

The precise size and shape of the NNLO corrections depend on the observable in question. However, all contributions are dominated by the behaviour in the two-jet region where the observable generally tends to zero. Of course, typical hadronic events contain many hadrons and it is extremely unlikely that the value of any event shape is precisely zero for any experimental event. However, in the fixed order partonic calculation, where

there are at most five partons present in the final state, one or more of the partons may be soft and/or collinear, and the observable may approach zero. In such circumstances, soft gluon singularities cause the fixed order prediction to become wildly unstable and grow logarithmically. In the infrared limit  $y \rightarrow 0$ , the perturbative coefficients have the following form,

$$\begin{aligned} y \frac{dA}{dy} &\sim A_1 L + A_0 \\ y \frac{dB}{dy} &\sim B_3 L^3 + B_2 L^2 + B_1 L + B_0 \\ y \frac{dC}{dy} &\sim C_5 L^5 + C_4 L^4 + C_3 L^3 + C_2 L^2 + C_1 L + C_0 \end{aligned} \quad (5.1)$$

where  $L = \ln(1/y)$  and  $C_n$  are (as yet) undetermined coefficients. Whenever  $L$  is sufficiently large, resummation effects will be important. In our numerical studies, we therefore impose a cut on the size of  $y$  which is typically in the range  $0.001 - 0.01$ , since for such small values of  $y$  we do not trust the fixed order prediction.

Even away from the infrared region, the shape of the fixed order prediction is heavily influenced by cancellations between the real and virtual contributions. The LO contribution  $A$  is very large and positive at small  $y$  and decreases monotonically as  $y$  increases. The NLO contribution  $B$  is negative at small  $y$ , but exhibits a turn-over, typically at  $y \sim 0.05$ . Similarly, the NNLO contribution  $C$  also exhibits a turn-over, but at a slightly larger value of  $y$ . The precise positions of the maxima of the distributions depend on the observable under consideration.

A second generic feature occurs when the paucity of final state particles imposes a maximum value for the observable. Examples include  $(1 - T)$  and  $C$  which are required to be less than 0.33 and 0.75 respectively for three-parton final states. As the number of partons increases with the perturbative order, this limit is relaxed and larger values of the observable are accessed.

Finally, typical values of the strong coupling constant lie around  $\alpha_s \sim 0.12$ , so that  $\frac{\alpha_s}{2\pi} \sim 1/50$ . It is well known that the NLO corrections are large,  $B_y \sim (15 - 30)A_y$ , leading to a 30-60% NLO effect in the region where the perturbative calculation is expected to be reliable. However, we observe that in all cases, the NNLO coefficients are also significant,  $C_y \sim (200 - 800)A_y$ , leading to a further 7-28% NNLO correction.

## 5.1 Thrust

Thrust is defined in section 2(a). First results for the NNLO corrections to the thrust distribution were presented in Ref. [46]. The perturbative coefficients for the thrust distribution weighted by  $(1 - T)$  are shown in Fig. 1. As discussed earlier, the shape of the contribution is dominated by the infrared region at  $(1 - T) \rightarrow 0$ . At small  $(1 - T)$ , the LO contribution  $A$  is very large and positive, while the NLO and NNLO coefficients  $B$  and  $C$  are rising and exhibit a turn-over at moderate values of  $(1 - T)$ . We observe that the peak moves from about 0.04 (NLO) to 0.06 (NNLO). We also see that the NLO and NNLO distributions progressively extend to larger and larger values of  $(1 - T)$  as the

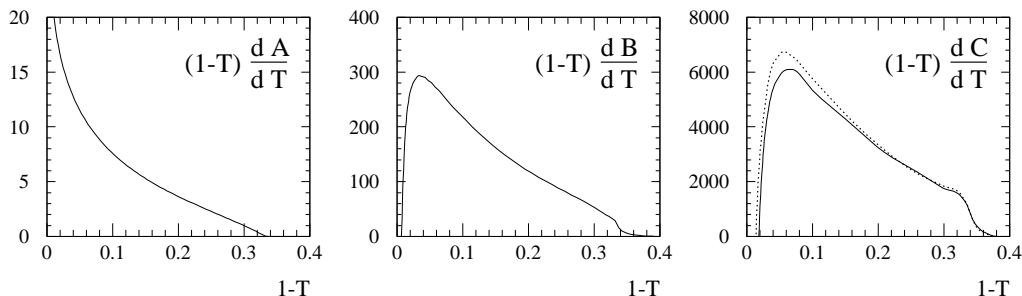


**Figure 1:** Coefficients of the leading order, next-to-leading order and next-to-next-to-leading order contributions to the thrust distribution as defined in Eq. (3.6) and weighted by  $(1 - T)$ . The dotted line in the  $C$  coefficient indicates the distribution prior to correction of the soft large-angle radiation terms (see erratum at the end of the paper).

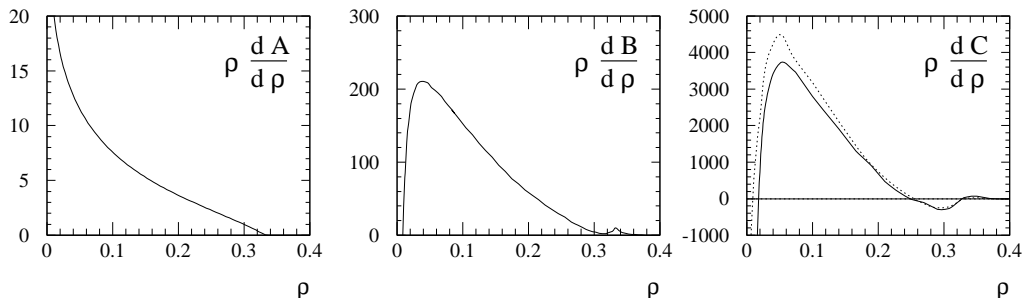


**Figure 2:** Coefficients of the leading order, next-to-leading order and next-to-next-to-leading order contributions to the heavy jet mass distribution as defined in Eq. (3.6) and weighted by  $\rho$ . The dotted line in the  $C$  coefficient indicates the distribution prior to correction of the soft large-angle radiation terms.

phase space restrictions on large values of  $(1 - T)$  are relaxed. In the intermediate region,  $0.04 < (1 - T) < 0.33$ , we observe that the perturbative coefficients are roughly in the ratio,  $A : B : C \sim 1 : 30 : 800$ . Setting  $\alpha_s \sim 0.12$  and using Eq. (3.7), this indicates corrections which are of relative magnitude  $\text{LO} : \text{NLO} : \text{NNLO} \sim 1 : 0.53 : 0.27$ , such that the NNLO corrections increase the NLO prediction by another 18%.

## 5.2 Heavy jet mass

The definition of the heavy jet mass given in section 2(b) is the larger invariant mass of the two hemispheres formed by separating the event by a plane normal to the thrust axis. The perturbative coefficients for the heavy jet mass distribution weighted by  $\rho$  are shown in Fig. 2. At lowest order, the heavy jet mass and the  $(1 - T)$  distribution are identical, so that  $A$  does not extend past  $\rho = 0.33$ . At higher orders, the distribution extends to larger values, with a small negative NNLO contribution around 0.33. In the intermediate region,  $0.02 < \rho < 0.33$ , the perturbative coefficients are roughly  $A : B : C \sim 1 : 20 : 400$  indicating corrections of approximately  $\text{LO} : \text{NLO} : \text{NNLO} \sim 1 : 0.34 : 0.13$ , translating into a 10% enhancement of NNLO over NLO. Comparing Fig. 1(b) with 2(b) and Fig. 1(c) with 2(c) we see clearly the rather different behaviour of the higher order corrections to these

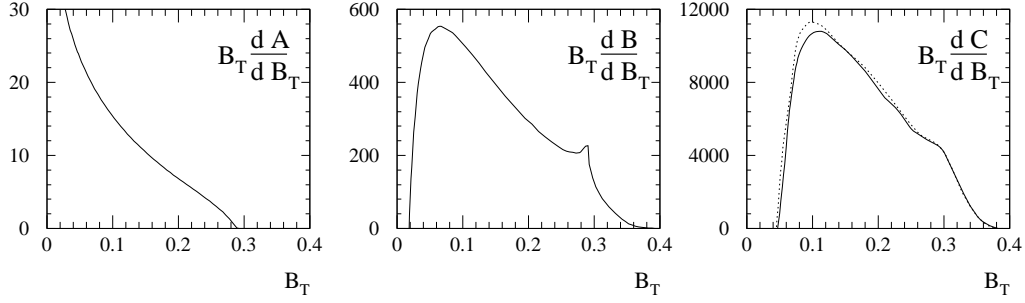


**Figure 3:** Coefficients of the leading order, next-to-leading order and next-to-next-to-leading order contributions to the total jet broadening distribution as defined in Eq. (3.6) and weighted by  $B_T$ . The dotted line in the  $C$  coefficient indicates the distribution prior to correction of the soft large-angle radiation terms.

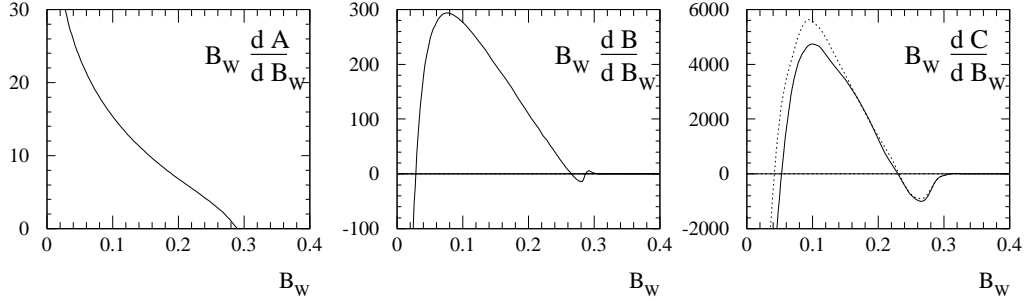


**Figure 4:** Coefficients of the leading order, next-to-leading order and next-to-next-to-leading order contributions to the wide jet broadening distribution as defined in Eq. (3.6) and weighted by  $B_W$ . The dotted line in the  $C$  coefficient indicates the distribution prior to correction of the soft large-angle radiation terms.

observables, particularly in the region beyond the LO kinematic bound where partonic configurations with two or more partons in each hemisphere contribute differently to each observable.

### 5.3 Jet broadenings

The jet broadenings are defined in section 2(c) by dividing the event into two hemispheres using a plane normal to the thrust axis.. At lowest order  $B_W$  and  $B_T$  are identical, but their distributions receive different higher order corrections from partonic configurations with two or more partons in each hemisphere.

The perturbative coefficients for the  $B_T$  ( $B_W$ ) distributions weighted by  $B_T$  ( $B_W$ ) are shown in Fig. 3 (Fig. 4) respectively. The structures evident around  $B_T$ ,  $B_W \sim (1/2\sqrt{3}) \sim 0.29$  are generated by four and five parton events and are therefore different for the two observables. For more moderate  $B_T$  values between 0.04 and 0.29, the perturbative coefficients are in the ratio  $A : B : C \sim 1 : 35 : 800$ . Including the factors of  $\alpha_s$ , this leads to corrections  $\text{LO} : \text{NLO} : \text{NNLO} \sim 1 : 0.63 : 0.27$  for  $\alpha_s \sim 0.12$ , which amounts to NNLO corrections of 17% of the NLO result. We observe that the corrections for  $B_W$

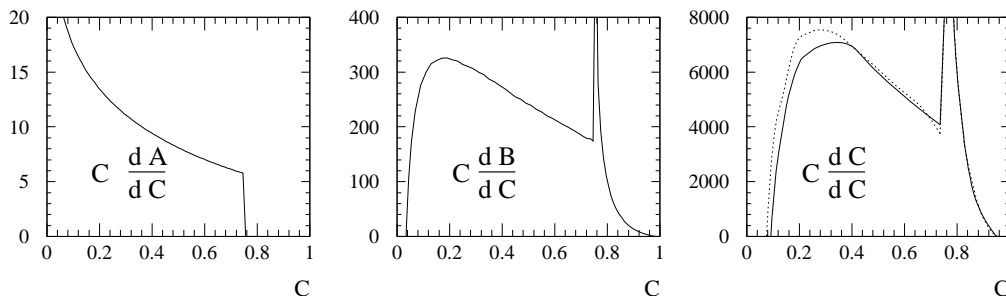


**Figure 5:** Coefficients of the leading order, next-to-leading order and next-to-next-to-leading order contributions to the  $C$  parameter distribution as defined in Eq. (3.6) and weighted by  $C$ . The dotted line in the  $C$  coefficient indicates the distribution prior to correction of the soft large-angle radiation terms.

are considerably smaller than those for  $B_T$ ,  $A : B : C \sim 1 : 20 : 400$  or equivalently  $LO : NLO : NNLO \sim 1 : 0.34 : 0.13$ , which yields a 10% NNLO effect over NLO. When  $B_T < 0.04$  ( $B_W < 0.04$ ), infrared logarithms must be resummed to produce a meaningful result.

#### 5.4 $C$ -parameter

The  $C$  parameter is defined in section 2(d) and the perturbative distributions at LO, NLO and NNLO weighted by  $C$  are shown in Fig. 5. The LO kinematic limit at  $C = 0.75$  is clearly visible. At NLO (and NNLO), four (and five) parton events can generate larger values of  $C$ , leading to a sharp peak around  $C \sim 0.75$ . The approximate size of the corrections for  $0.1 < C < 0.75$  is  $A : B : C \sim 1 : 30 : 700$ , or, including the factors of  $(\alpha_s/2\pi)$  with  $\alpha_s \sim 0.12$ , in the ratio  $LO : NLO : NNLO \sim 1 : 0.53 : 0.23$ , resulting in a 15% enhancement of NNLO over NLO. At smaller values of  $C < 0.1$ , large infrared logarithms render the fixed order prediction unreliable and must be resummed. Similarly, large logarithms are produced around the LO kinematic limit,  $C \sim 0.75$  which must also be resummed.

#### 5.5 $Y_3$

The jet transition variable  $Y_3$  is defined in section 2(e). It describes the value of the jet resolution parameter  $y_{\text{cut}}$  for which an event changes from a three-jet to a two-jet configuration within the Durham jet algorithm. The perturbative distributions at LO, NLO and NNLO weighted by  $Y_3$  are shown in Fig. 5. As with all of the event shapes,  $Y_3 dA/dY_3$  is linear when plotted on a logarithmic scale. For moderate values of  $Y_3$ ,  $2 < -\ln(Y_3) < 6$ , the corrections are positive. In this region, the approximate size of the corrections is  $A : B : C \sim 1 : 15 : 200$ , or, including the factors of  $(\alpha_s/2\pi)$  with  $\alpha_s \sim 0.12$ , in the ratio  $LO : NLO : NNLO \sim 1 : 0.25 : 0.06$ , which produces a 5% NNLO effect over NLO. However, at smaller values of  $Y_3$  (larger values of  $-\ln(Y_3)$ ) resummation of logarithmic contributions are clearly mandatory.

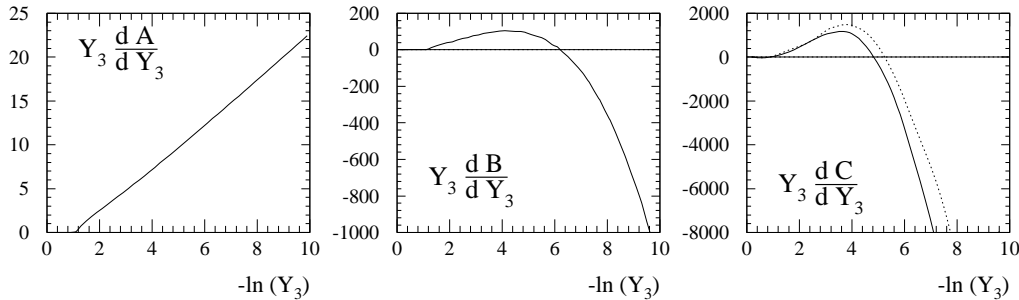


**Figure 6:** Coefficients of the leading order, next-to-leading order and next-to-next-to-leading order contributions to the distribution of the jet transition variable  $Y_3$  as defined in Eq. (3.6) and weighted by  $Y_3$ . The dotted line in the  $C$  coefficient indicates the distribution prior to correction of the soft large-angle radiation terms.

## 6. Comparison with data

We have presented the NNLO corrections to six event-shape distributions. As we have shown in the previous section, the magnitude of the NNLO correction is different for the six variables.

Each of the event shapes considered here has been studied in depth by all four experiments at LEP at centre-of-mass energies of 91.2, 133, 161, 172, 183, 189, 200 and 206 GeV [1–4]. Within the experimental uncertainties, these data sets are mutually consistent.

In this paper, we select data from ALEPH [1] as a representative set of hadronic final states in electron-positron annihilation to illustrate the improvement in the theoretical prediction due to the inclusion of the NNLO perturbative contribution. The only free parameter in our predictions is the strong coupling constant; we use the current world average value  $\alpha_s(M_Z) = 0.1189$  [47].

The experimental event-shape distributions were computed using the reconstructed momenta and energies of charged and neutral particles. The measurements have been corrected for detector effects and the final distributions correspond to the particle (or hadron) level (stable hadrons and leptons after hadronisation). In addition, at LEP2 energies above the  $Z$  peak the data were corrected for initial-state radiation effects and backgrounds, mainly from  $W$ -pair production, were subtracted. The experimental uncertainties were estimated by varying event and particle selection cuts and are below 1% at LEP1 and between 0.5% and 1.5% at LEP2. For further details we refer the interested reader to Ref. [1].

### 6.1 Thrust

Figure 7 displays the perturbative expression for the thrust distribution<sup>2</sup> at LO, NLO and NNLO, evaluated at  $Q = M_Z$ . The error band indicates the variation of the prediction under shifts of the renormalisation scale in the range  $\mu \in [Q/2; 2Q]$  around the  $e^+e^-$  centre-of-mass energy  $Q$ . The relative scale uncertainty is reduced by about 30% between NLO and NNLO.

<sup>2</sup>First results for the NNLO corrections to the thrust distribution were presented in Ref. [46]

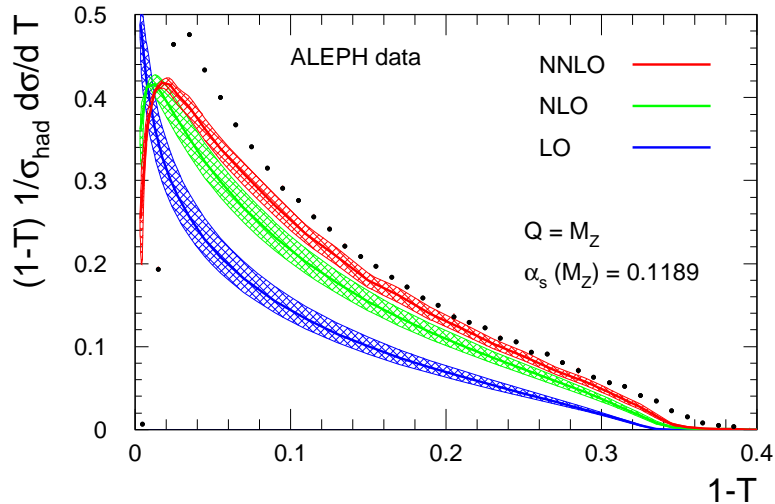


**Figure 7:** Thrust distribution at  $Q = M_Z$  at LO (blue), NLO (green) and NNLO (red). The solid lines represent the prediction for renormalisation scale  $\mu = Q$  and  $\alpha_s(M_Z) = 0.1189$ , while the shaded region shows the variation due to varying the renormalisation scale between  $\mu = Q/2$  and  $\mu = 2Q$ . The data is taken from [1].

The inclusion of the NNLO corrections enhances the thrust distribution by around (15-20)% over the range  $0.04 < (1 - T) < 0.33$ , where  $-\ln(1 - T)$  is not too large. Outside this range, one does not expect the perturbative fixed-order prediction to yield reliable results. For  $(1 - T) \rightarrow 0$ , the convergence of the perturbative series is spoilt by powers of logarithms  $\ln(1 - T)$  appearing in higher perturbative orders, thus necessitating an all-order resummation of these logarithmic terms [10, 11], and a matching of fixed-order and resummed predictions [48].

The perturbative parton-level prediction is compared with the hadron-level data from the ALEPH collaboration [1] in Figure 7 and Figure 8. We observe that for all  $Q$  values, the shape and normalisation of the parton level NNLO prediction agrees better with the data than at NLO. We also see that the NNLO corrections account for approximately half of the difference between the parton-level NLO prediction and the hadron-level data.

## 6.2 Heavy jet mass

The perturbative prediction for the heavy jet mass distribution is displayed in Figure 9. The solid lines represent the prediction at the physical scale  $Q = M_Z$ , while the shaded bands represent the effect of varying the renormalisation scale upwards and downwards by a factor of 2. We observe that the relative scale uncertainty is reduced by about 50% between NLO and NNLO. It is noteworthy that the original motivation for introducing the heavy jet mass distribution [20] was the hope for improved perturbative stability over the thrust distribution. This improved stability was not evident from the existing NLO results alone, but becomes visible at NNLO.

Compared to NLO, the inclusion of the NNLO corrections enhances the heavy jet mass distribution by around 10% over the range  $0.02 < \rho < 0.33$ , where  $\ln(\rho)$  is not too



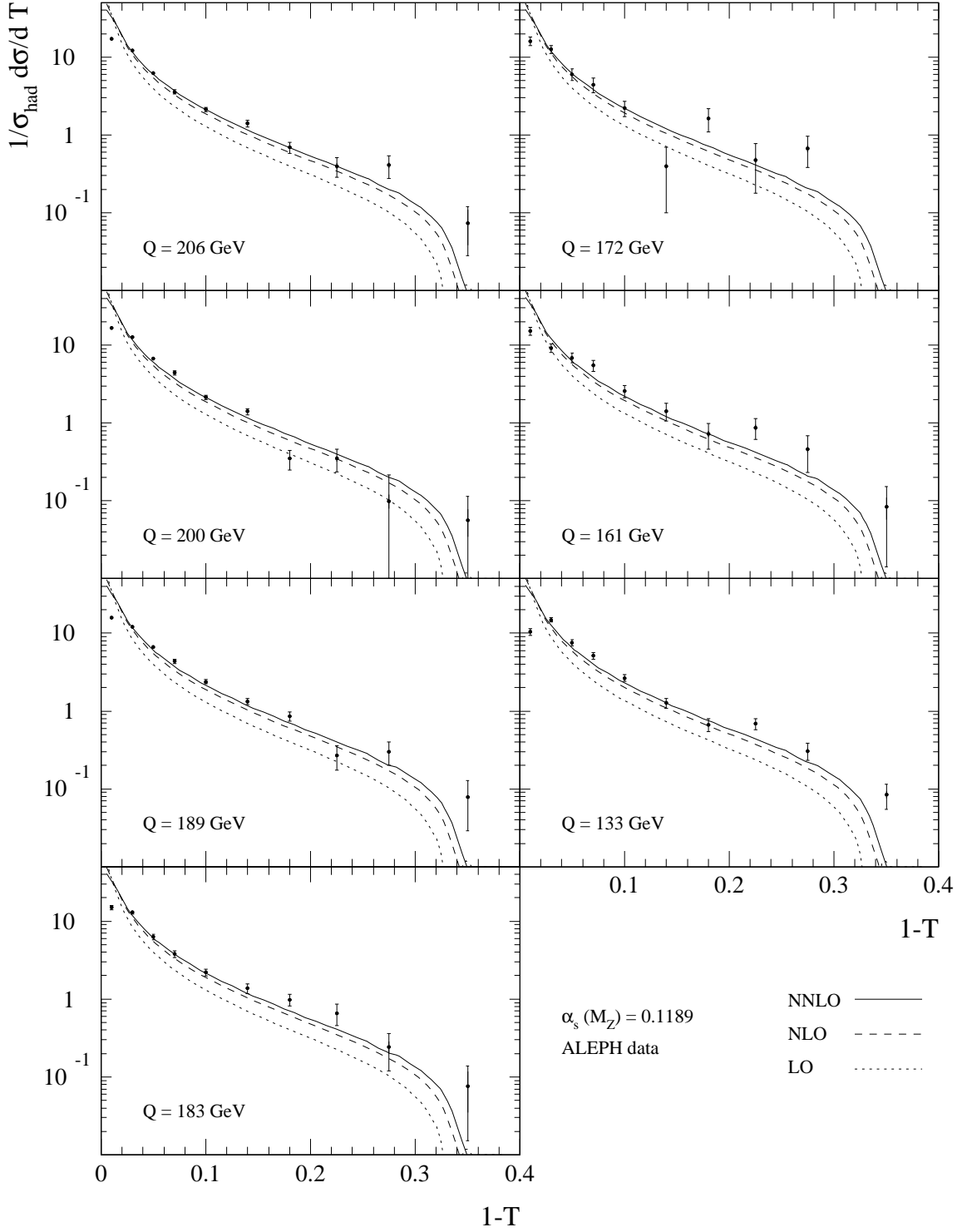


**Figure 8:** The thrust distribution (with  $\mu = Q$  and  $\alpha_s(M_Z) = 0.1189$ ) at LO (dotted), NLO (dashed) and NNLO (solid) compared to experimental data from ALEPH [1] for  $Q = 133 \text{ GeV}, \dots, 206 \text{ GeV}$ .

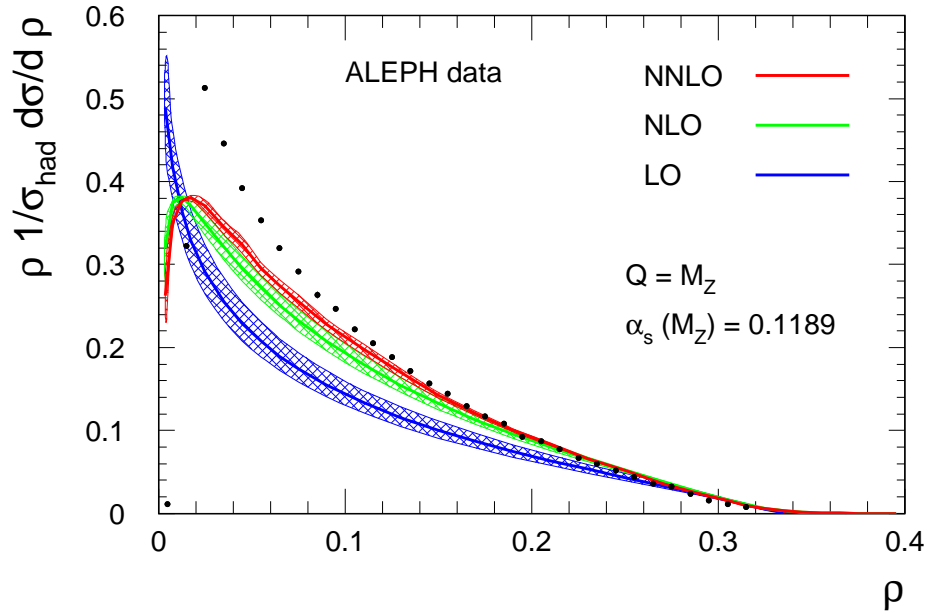


**Figure 9:** Heavy jet mass distribution at  $Q = M_Z$  at LO (blue), NLO (green) and NNLO (red). The solid lines represent the prediction for renormalisation scale  $\mu = Q$  and  $\alpha_s(M_Z) = 0.1189$ , while the shaded region shows the variation due to varying the renormalisation scale between  $\mu = Q/2$  and  $\mu = 2Q$ . The data is taken from [1].

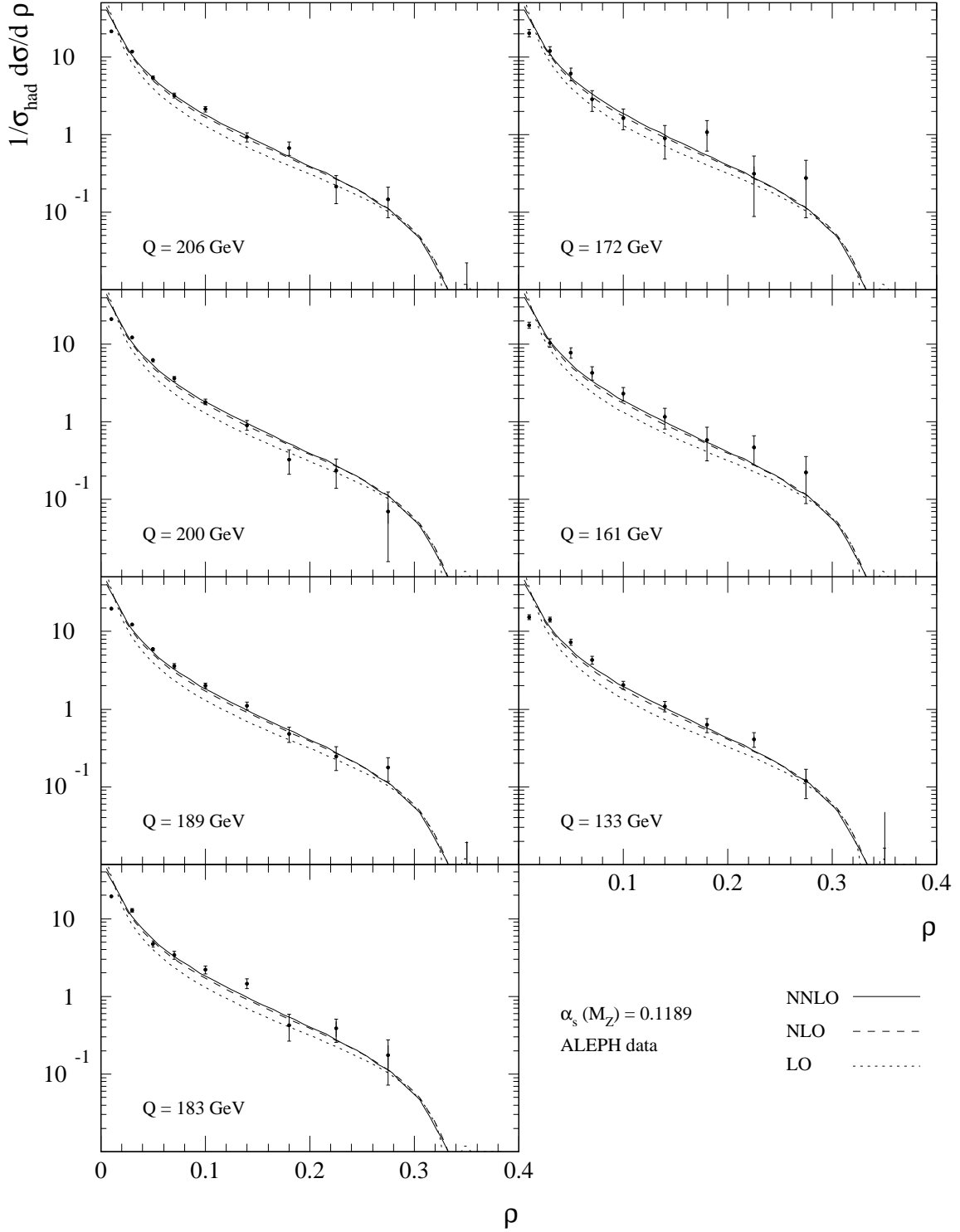
large. At smaller  $\rho$  values, large  $\ln(1/\rho)$  corrections must be resummed to all orders [49] and matched onto the perturbative prediction. Nevertheless, in the moderate to large  $\rho$  region, the NNLO corrections render the fixed order prediction significantly closer to the experimental data [1].

Figure 10 shows the prediction for a range of  $Q$  values together with the hadron-level data from the ALEPH collaboration [1]. For this observable, the NNLO corrections are relatively small, however, for all  $Q$  values, the shape and normalisation of the parton-level NNLO prediction agrees slightly better with the hadron-level data than at NLO.

### 6.3 Jet broadenings

Predictions for the total and wide jet broadenings are displayed in Figures 11 and 12. The solid lines represent the prediction at the physical scale  $Q = M_Z$ , while the shaded bands represent the effect of varying the renormalisation scale upwards and downwards by a factor of 2. We observe that the relative scale uncertainty in the  $B_T$  ( $B_W$ ) distribution is reduced by about 40% (50%) between NLO and NNLO.

As anticipated from the discussion in section 5.3, we observe that the perturbative corrections are smaller for  $B_W$  than for  $B_T$ . In the region where perturbation theory is expected to yield reliable results,  $(B_T, B_W) > 0.05$ , we observe an enhancement of (15-20)% in  $B_T$  and of (8-12)% in  $B_W$ . As with  $(1 - T)$  and the heavy jet mass, the two broadenings are identical at leading order, but display a largely different behaviour in the higher perturbative corrections. At smaller values of broadening, large logarithmic corrections occur which must be resummed [21].



**Figure 10:** Heavy jet mass distribution (with  $\mu = Q$  and  $\alpha_s(M_Z) = 0.1189$ ) at LO (dotted), NLO (dashed) and NNLO (solid) compared to experimental data from ALEPH [1] for  $Q = 133$  GeV, ..., 206 GeV.

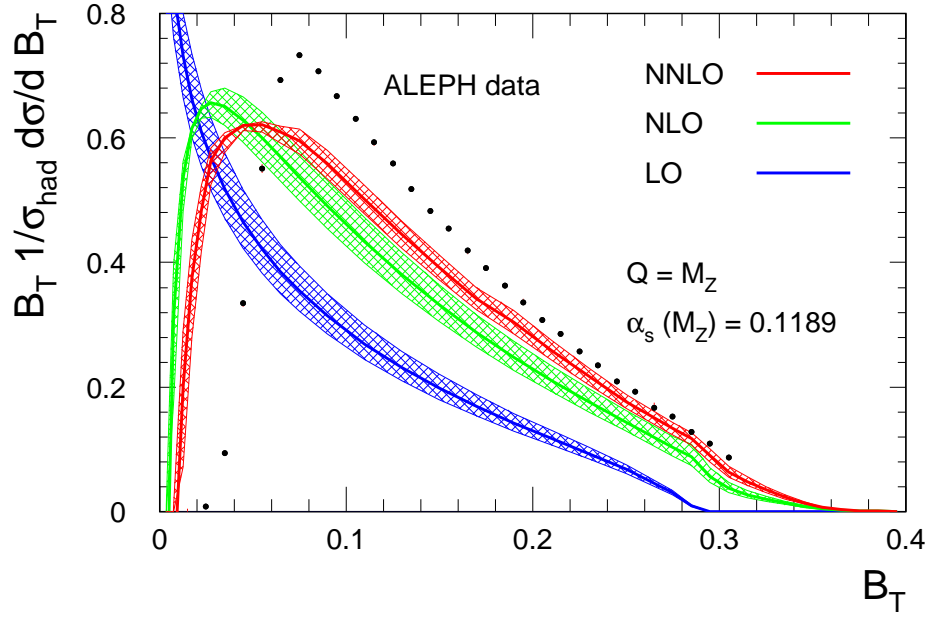


**Figure 11:** Total jet broadening distribution at  $Q = M_Z$  at LO (blue), NLO (green) and NNLO (red). The solid lines represent the prediction for renormalisation scale  $\mu = Q$  and  $\alpha_s(M_Z) = 0.1189$ , while the shaded region shows the variation due to varying the renormalisation scale between  $\mu = Q/2$  and  $\mu = 2Q$ . The data is taken from [1].

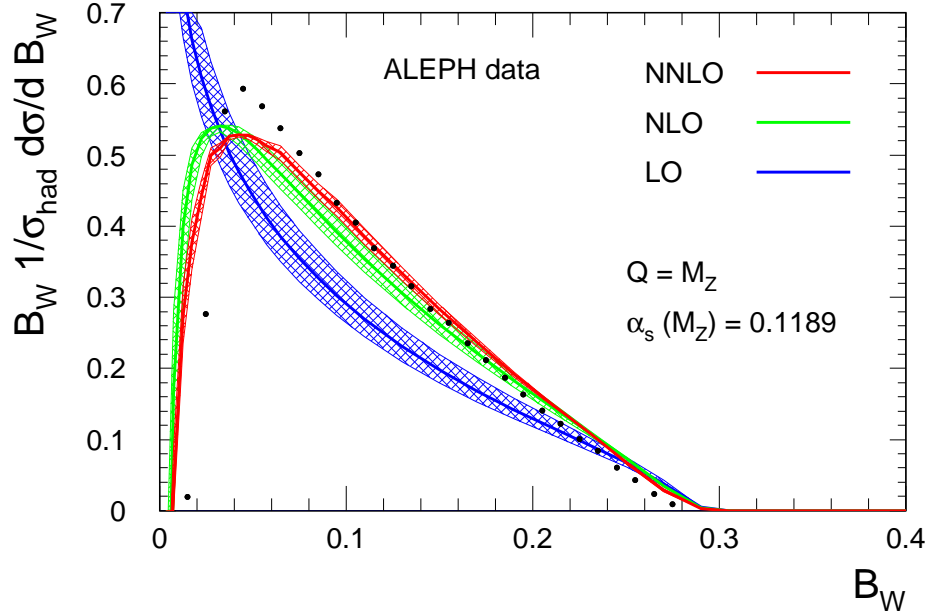


**Figure 12:** Wide jet broadening distribution at  $Q = M_Z$  at LO (blue), NLO (green) and NNLO (red). The solid lines represent the prediction for renormalisation scale  $\mu = Q$  and  $\alpha_s(M_Z) = 0.1189$ , while the shaded region shows the variation due to varying the renormalisation scale between  $\mu = Q/2$  and  $\mu = 2Q$ . The data is taken from [1].

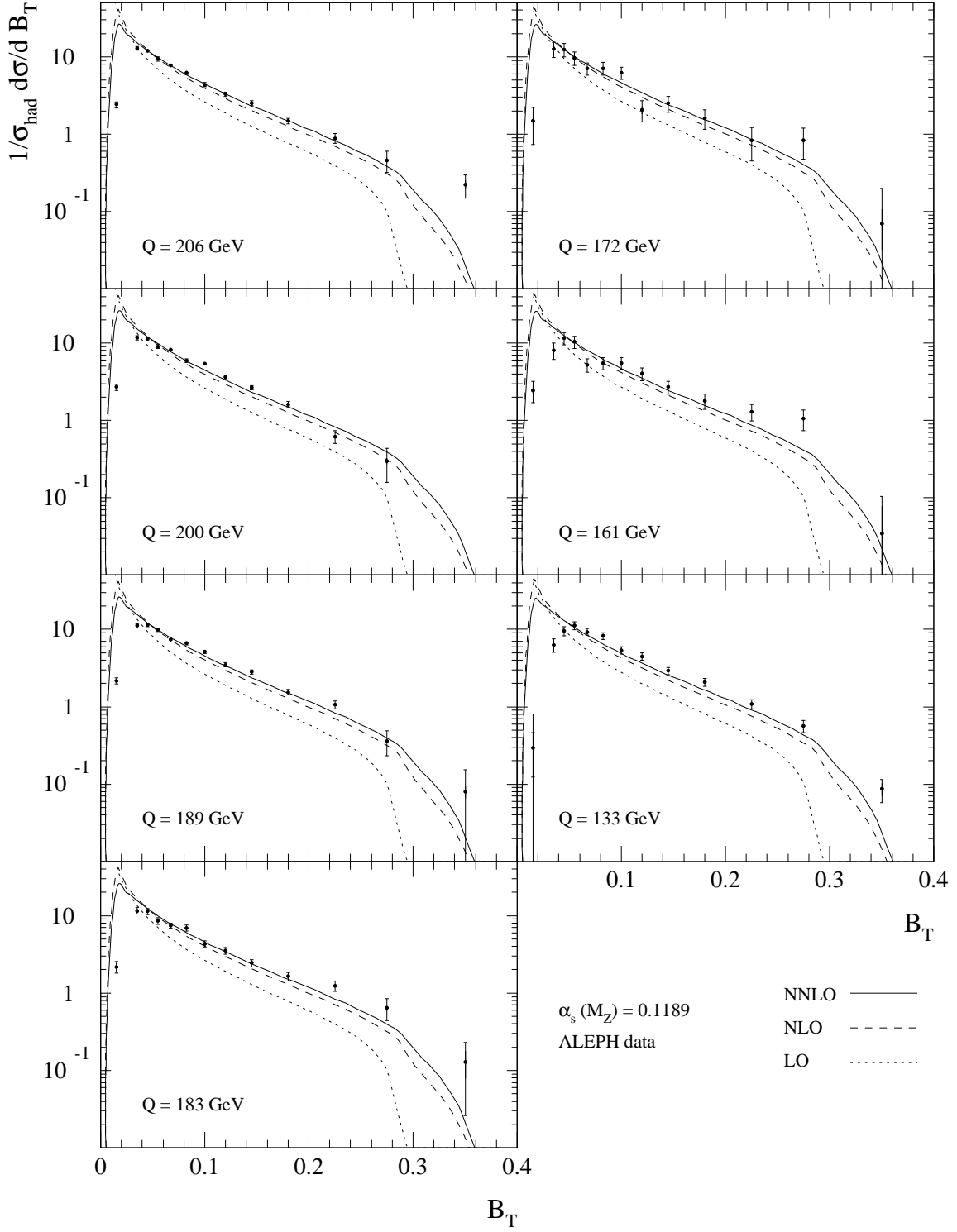


**Figure 13:** Total jet broadening distribution (with  $\mu = Q$  and  $\alpha_s(M_Z) = 0.1189$ ) at LO (dotted), NLO (dashed) and NNLO (solid) compared to experimental data from ALEPH [1] for  $Q = 133 \text{ GeV}, \dots, 206 \text{ GeV}$ .

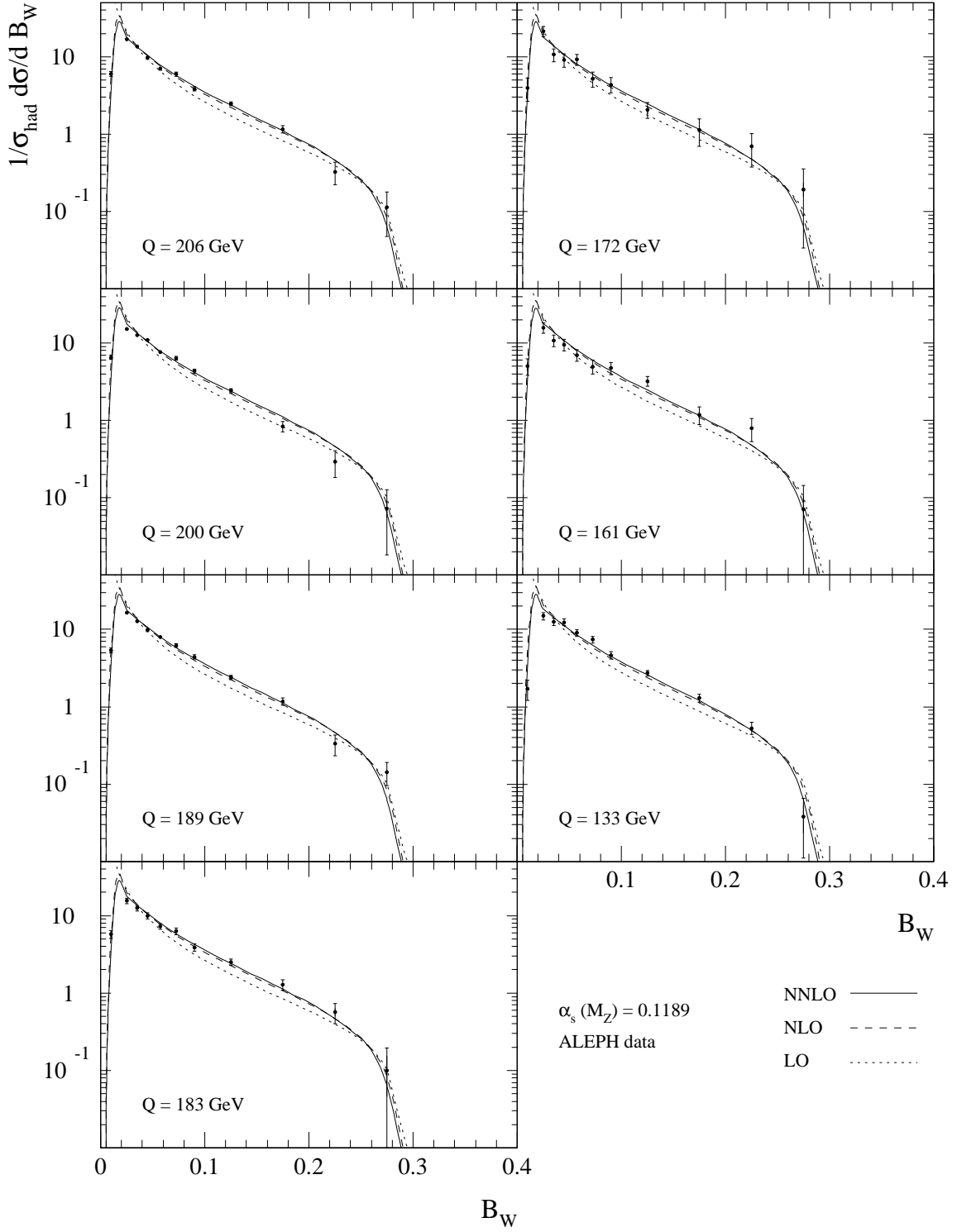


**Figure 14:** Wide jet broadening distribution (with  $\mu = Q$  and  $\alpha_s(M_Z) = 0.1189$ ) at LO (dotted), NLO (dashed) and NNLO (solid) compared to experimental data from ALEPH [1] for  $Q = 133 \text{ GeV}, \dots, 206 \text{ GeV}$ .

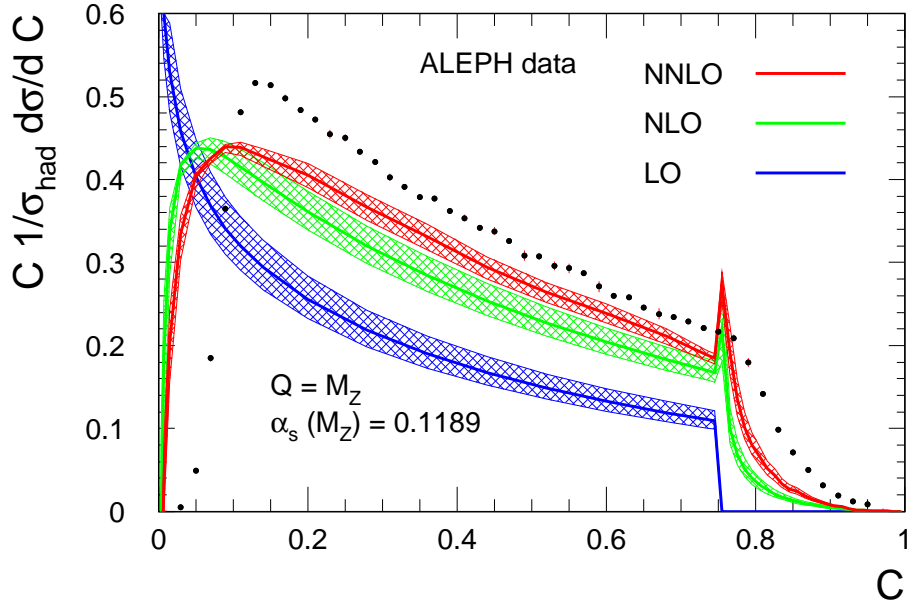


**Figure 15:**  $C$  parameter distribution at  $Q = M_Z$  at LO (blue), NLO (green) and NNLO (red). The solid lines represent the prediction for renormalisation scale  $\mu = Q$  and  $\alpha_s(M_Z) = 0.1189$ , while the shaded region shows the variation due to varying the renormalisation scale between  $\mu = Q/2$  and  $\mu = 2Q$ . The data is taken from [1].

To guide the eye, Figures 11 and 12 also show hadron-level data from the ALEPH collaboration [1]. For both broadenings, we see that the NNLO prediction lies closer to the data, and, in fact, accounts for much of the difference between the NLO prediction and the hadron-level data.

The experiments at LEP also gathered data at higher  $Q$  values; Figures 13 and 14 compare the parton-level prediction at  $Q = 133 \text{ GeV}, \dots, 206 \text{ GeV}$  with hadron-level data from the ALEPH collaboration [1]. We observe that for all  $Q$  values, shape and normalisation of the parton level NNLO prediction agrees better with the data than at NLO.

#### 6.4 $C$ -parameter

The  $C$  parameter is one of the classic event shape observables and we display the perturbative prediction in Figure 15. The solid lines represent the prediction at the physical scale  $Q = M_Z$ , while the shaded bands represent the effect of varying the renormalisation scale upwards and downwards by a factor of 2. We observe that the relative scale uncertainty is reduced by about 40% between NLO and NNLO. The NNLO corrections enhance the  $C$  parameter distribution by around (12-20)% over the range  $0.1 < C < 0.75$ , where  $\ln(1/C)$  is not too large. Figure 15 also shows hadron-level data from the ALEPH collaboration [1] and we observe that the NNLO parton-level prediction lies significantly closer to the data, and in fact, accounts for about one third of the difference between the NLO prediction and the data.

At small  $C$ , one expects large logarithmic contributions  $\ln(1/C)$  appearing in higher perturbative orders, thus necessitating an all-orders resummation of these logarithmic

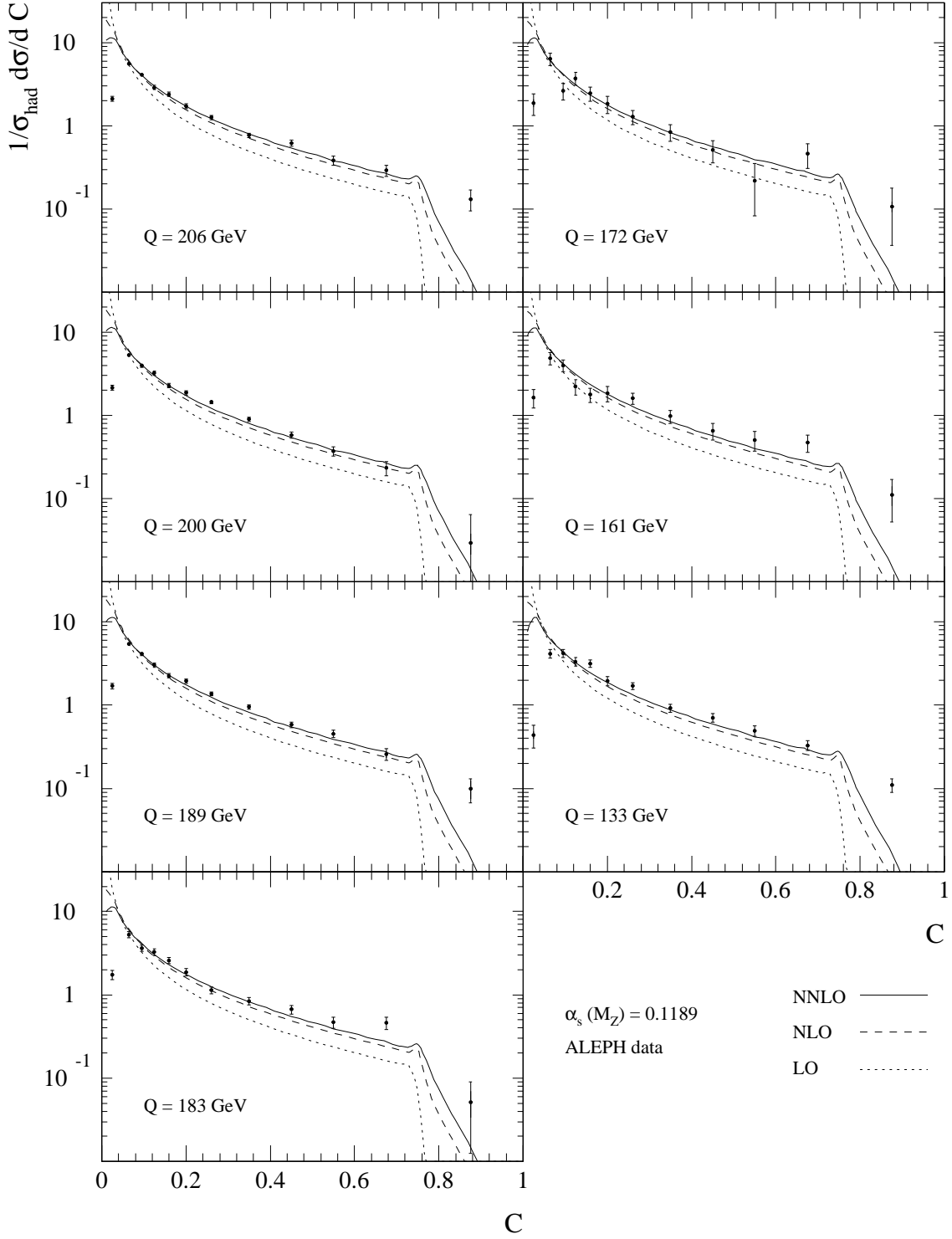


**Figure 16:** C parameter distribution (with  $\mu = Q$  and  $\alpha_s(M_Z) = 0.1189$ ) at LO (dotted), NLO (dashed) and NNLO (solid) compared to experimental data from ALEPH [1] for  $Q = 133 \text{ GeV}, \dots, 206 \text{ GeV}$ .



terms [50]. There are also large logarithms around  $C \sim 0.75$ , due to soft gluon divergences within the physical region (producing a so-called Sudakov shoulder in the distribution) which must also be resummed [51] to all orders.

Figure 16 shows the prediction for a range of  $Q$  values together with the hadron-level data from the ALEPH collaboration [1]. For all  $Q$  values, the shape and normalisation of the parton level NNLO prediction agrees slightly better with the data than at NLO.

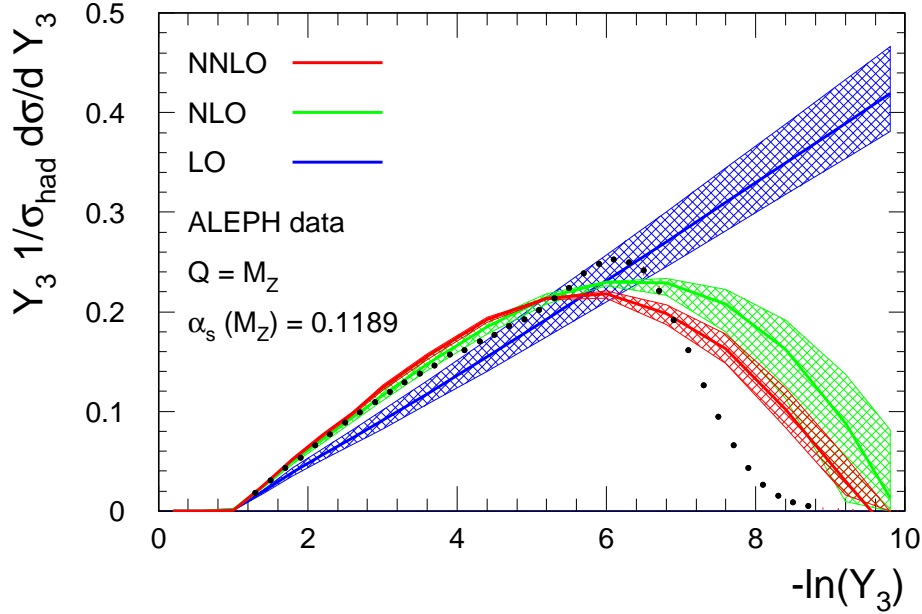


**Figure 17:** The distribution for the jet transition variable,  $Y_3$  at  $Q = M_Z$  at LO (blue), NLO (green) and NNLO (red). The solid lines represent the prediction for renormalisation scale  $\mu = Q$  and  $\alpha_s(M_Z) = 0.1189$ , while the shaded region shows the variation due to varying the renormalisation scale between  $\mu = Q/2$  and  $\mu = 2Q$ . The data is taken from [1].

### 6.5 $Y_3$

Figure 17 displays the perturbative expression for the  $Y_3$  distribution at LO, NLO and NNLO, evaluated at  $Q = M_Z$ . The error band indicates the variation of the prediction under shifts of the renormalisation scale in the range  $\mu \in [Q/2; 2Q]$  around the  $e^+e^-$  centre-of-mass energy  $Q$ . The relative scale uncertainty is reduced by about 50% between NLO and NNLO.

The NLO and NNLO corrections change the shape of the distribution considerably and introduce a turnover at  $-\ln(Y_3) \sim 5 - 6$ . We observe that the NNLO corrections modify the  $Y_3$  distribution by around (3-5)% over the range  $2 < -\ln(Y_3) < 6$ , where  $-\ln(Y_3)$  is moderate. At larger  $-\ln(Y_3)$ , one does not expect fixed-order perturbation theory to yield reliable results and the large infrared logarithms of the type  $\alpha_s^n \ln^m(Y_3)$  must be resummed [52].

The perturbative parton-level prediction is compared with the hadron-level data from the ALEPH collaboration [1] in Figure 17 and Figure 18. We see that the quality of the

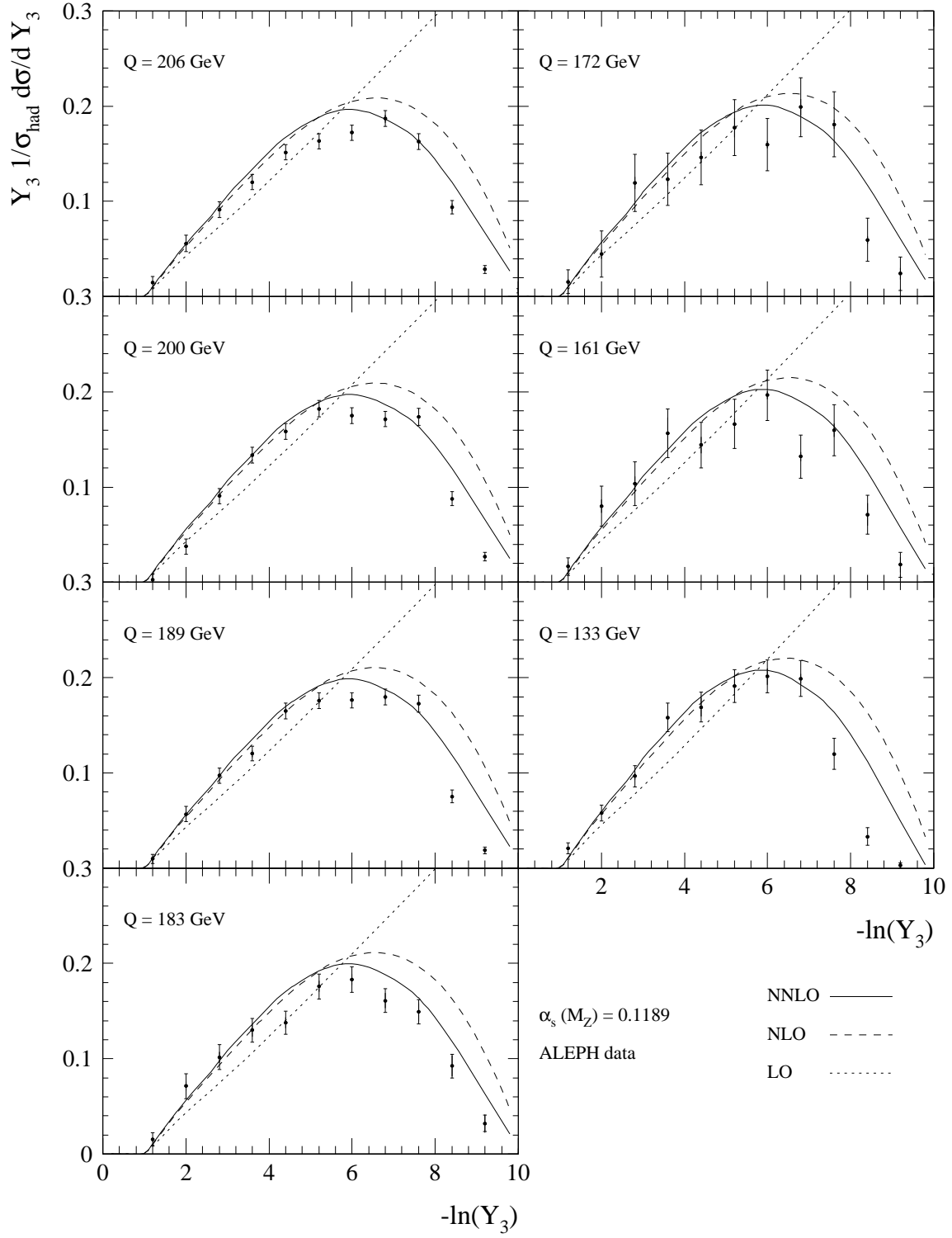


**Figure 18:** The  $Y_3$  distribution (with  $\mu = Q$  and  $\alpha_s(M_Z) = 0.1189$ ) at LO (dotted), NLO (dashed) and NNLO (solid) compared to experimental data from ALEPH [1] for  $Q = 133$  GeV, ..., 206 GeV.

agreement between fixed order perturbation theory and data is much more  $Q$  dependent than for the other observables considered in this paper. At  $Q = M_Z$ , the data is much more sharply peaked than the NNLO prediction. However, at higher  $Q$  values shown in Figure 18, the agreement between the NNLO prediction and the data around the peak region is very good - and significantly better than at NLO.

## 7. Conclusions and Outlook

The main goal of this paper is to provide improved theoretical predictions for hadronic event shape observables in electron-positron annihilation. To this end, we have presented new results for the next-to-next-to-leading order contributions to a number of important three-jet-like event shape observables in  $e^+e^-$  collisions. These results are obtained using a numerical program, that is based on the matrix elements for  $\gamma^* \rightarrow 3$  partons at two-loop,  $\gamma^* \rightarrow 4$  partons at one-loop and  $\gamma^* \rightarrow 5$  partons at tree-level. Each of these contributions becomes singular when one or more partons are soft and/or collinear, and we have developed and implemented an NNLO subtraction formalism to subtract these singularities, thereby yielding a finite NNLO prediction. The resulting numerical program, **EERAD3**, yields the full kinematical information on the partonic final state and can be applied to generic infrared safe three-jet observables.

For the six event shapes considered here, and in kinematical regions where infrared logarithms are small enough to render their resummation unnecessary, the NLO corrections are generally large - of the order 30-60%. The NNLO effects produce a further 5-20% correction. Comparisons with existing data from LEP indicate an improved agreement with hadronic data and the fixed order NNLO parton-level prediction. In addition, the remaining theoretical uncertainty estimated by varying the renormalisation scale by a factor of two around the physical scale is also significantly reduced, typically by 30-50%. Importantly, the size of the corrections is different for different observables.

Our results for the NNLO corrections open up a whole new range of possible comparisons with the LEP data. For meaningful comparisons, one has to account for hadronisation effects, either by introducing hadron-level to parton-level correction factors, or by including power-suppressed hadronisation effects in the theoretical description. A first direct determination of the strong coupling constant from a fit of next-to-next-to-leading order QCD predictions to event-shape variables over a range of  $Q$  values will be reported in a separate publication [53] and should yield a much more precise value of  $\alpha_s(M_Z)$  than that previously extracted from event shapes. Our predictions can be further improved by a NLL resummation of the large infrared logarithms that are present as  $y \rightarrow 0$ . The ingredients for  $\ln R$  matching to NNLO are available in [11]. Studies in this direction are in progress and should yield a further improvement on the measurement of  $\alpha_s(M_Z)$ . Similarly, our results will also allow a renewed study of power corrections, now matched to NNLO.

## Acknowledgements

We would like to thank Günther Dissertori and Hasko Stenzel for sharing their expertise

on QCD event shapes in many useful discussions.

Part of this work was carried out while the authors were attending the programme “Advancing Collider Physics: From Twistors to Monte Carlos” of the Galileo Galilei Institute for Theoretical Physics (GGI) in Florence. We thank the GGI for its hospitality and the Istituto Nazionale di Fisica Nucleare (INFN) for partial support.

This research was supported in part by the Swiss National Science Foundation (SNF) under contract 200020-117602, by the UK Science and Technology Facilities Council and by the European Commission’s Marie-Curie Research Training Network under contract MRTN-CT-2006-035505 “Tools and Precision Calculations for Physics Discoveries at Colliders”.

## Erratum added

Our implementation of NNLO corrections to three-jet-like observables [17], which was used for the present work, was checked by two subsequent studies: the calculation of all logarithmically enhanced contributions to the thrust distribution by Becher and Schwartz [A], and an independent implementation of our subtraction formulae by Weinzierl [B].

These works uncovered numerical discrepancies in the two-jet limit of the observables in two of the six colour factor contributions:  $N^2$  and  $N^0$ . In [B], it was shown that the origin of these discrepancies is in an oversubtraction of large-angle soft radiation. We described the corrected treatment of these terms in the erratum to [17].

As a consequence, the numerical values of the NNLO coefficients of all event shape distributions were modified. The new coefficients are displayed by the solid lines in Figures 1–6, our original results are displayed there for comparison as dotted lines. It can be seen that in the genuine three-jet region, which is relevant for precision phenomenology, the changes have a minor numerical impact. The modification to the full event shape distributions is too small to be visible, except for  $Y_3$  in the deep two-jet region. We therefore refrain from presenting revised figures 7–18.

## References

- [1] D. Buskulic *et al.* [ALEPH Collaboration], Z. Phys. C **73** (1997) 409;  
A. Heister *et al.* [ALEPH Collaboration], Eur. Phys. J. C **35** (2004) 457.
- [2] P. Abreu *et al.* [DELPHI Collaboration], Phys. Lett. B **456** (1999) 322;  
J. Abdallah *et al.* [DELPHI Collaboration], Eur. Phys. J. C **29** (2003) 285 [hep-ex/0307048];  
J. Abdallah *et al.* [DELPHI Collaboration], Eur. Phys. J. C **37** (2004) 1 [hep-ex/0406011].
- [3] M. Acciarri *et al.* [L3 Collaboration], Phys. Lett. B **371** (1996) 137;  
M. Acciarri *et al.* [L3 Collaboration], Phys. Lett. B **404** (1997) 390;  
M. Acciarri *et al.* [L3 Collaboration], Phys. Lett. B **444** (1998) 569;  
P. Achard *et al.* [L3 Collaboration], Phys. Lett. B **536** (2002) 217 [hep-ex/0206052];  
P. Achard *et al.* [L3 Collaboration], Phys. Rept. **399** (2004) 71 [hep-ex/0406049].
- [4] P. D. Acton *et al.* [OPAL Collaboration], Z. Phys. C **59** (1993) 1;  
G. Alexander *et al.* [OPAL Collaboration], Z. Phys. C **72** (1996) 191;  
K. Ackerstaff *et al.* [OPAL Collaboration], Z. Phys. C **75** (1997) 193;

- G. Abbiendi *et al.* [OPAL Collaboration], Eur. Phys. J. C **16** (2000) 185 [hep-ex/0002012];  
G. Abbiendi *et al.* [OPAL Collaboration], Eur. Phys. J. C **40** (2005) 287 [hep-ex/0503051].
- [5] K. Abe *et al.* [SLD Collaboration], Phys. Rev. D **51** (1995) 962 [hep-ex/9501003].
- [6] O. Biebel, Phys. Rept. **340** (2001) 165;  
S. Kluth, Rept. Prog. Phys. **69** (2006) 1771.
- [7] R.K. Ellis, D.A. Ross and A.E. Terrano, Nucl. Phys. B **178** (1981) 421.
- [8] Z. Kunszt, Phys. Lett. B **99** (1981) 429;  
J.A.M. Vermaseren, K.J.F. Gaemers and S.J. Oldham, Nucl. Phys. B **187** (1981) 301;  
K. Fabricius, I. Schmitt, G. Kramer and G. Schierholz, Z. Phys. C **11** (1981) 315.
- [9] Z. Kunszt and P. Nason, in *Z Physics at LEP 1*, CERN Yellow Report 89-08, Vol. 1, p. 373;  
W. T. Giele and E.W.N. Glover, Phys. Rev. D **46** (1992) 1980;  
S. Catani and M. H. Seymour, Phys. Lett. B **378** (1996) 287 [hep-ph/9602277].
- [10] S. Catani, G. Turnock, B.R. Webber and L. Trentadue, Phys. Lett. B **263** (1991) 491.
- [11] S. Catani, L. Trentadue, G. Turnock and B.R. Webber, Nucl. Phys. B **407** (1993) 3.
- [12] G.P. Korchemsky and G. Sterman, Nucl. Phys. B **437** (1995) 415; Y.L. Dokshitzer and  
B.R. Webber, Phys. Lett. B **352** (1995) 451; **404** (1997) 321; Y.L. Dokshitzer, A. Lucenti,  
G. Marchesini and G.P. Salam, JHEP **9805** (1998) 003.
- [13] L.W. Garland, T. Gehrmann, E.W.N. Glover, A. Koukoutsakis and E. Remiddi, Nucl. Phys.  
B **627** (2002) 107 [hep-ph/0112081] and **642** (2002) 227 [hep-ph/0206067].
- [14] E.W.N. Glover and D.J. Miller, Phys. Lett. B **396** (1997) 257 [hep-ph/9609474];  
Z. Bern, L.J. Dixon, D.A. Kosower and S. Weinzierl, Nucl. Phys. B **489** (1997) 3  
[hep-ph/9610370];  
J.M. Campbell, E.W.N. Glover and D.J. Miller, Phys. Lett. B **409** (1997) 503  
[hep-ph/9706297];  
Z. Bern, L.J. Dixon and D.A. Kosower, Nucl. Phys. B **513** (1998) 3 [hep-ph/9708239].
- [15] K. Hagiwara and D. Zeppenfeld, Nucl. Phys. B **313** (1989) 560;  
F.A. Berends, W.T. Giele and H. Kuijf, Nucl. Phys. B **321** (1989) 39;  
N.K. Falck, D. Graudenz and G. Kramer, Nucl. Phys. B **328** (1989) 317.
- [16] A. Gehrmann-De Ridder, T. Gehrmann and E.W.N. Glover, JHEP **0509** (2005) 056  
[hep-ph/0505111]; Phys. Lett. B **612** (2005) 36 [hep-ph/0501291]; **612** (2005) 49  
[hep-ph/0502110].
- [17] A. Gehrmann-De Ridder, T. Gehrmann, E.W.N. Glover and G. Heinrich, JHEP **0711** (2007)  
058 [arXiv:0710.0346 [hep-ph]].
- [18] R.K. Ellis, W.J. Stirling and B.R. Webber, *QCD and Collider Physics*, Cambridge University  
Press (Cambridge, 1996);  
G. Dissertori, I.G. Knowles and M. Schmelling, *Quantum Chromodynamics: High Energy  
Experiments and Theory*, Oxford University Press (Oxford, 2003).
- [19] S. Brandt, C. Peyrou, R. Sosnowski and A. Wroblewski, Phys. Lett. **12** (1964) 57; E. Farhi,  
Phys. Rev. Lett. **39** (1977) 1587.
- [20] L. Clavelli and D. Wyler, Phys. Lett. B **103** (1981) 383.

- [21] P.E.L. Rakow and B.R. Webber, Nucl. Phys. B **191** (1981) 63;  
S. Catani, G. Turnock and B. R. Webber, Phys. Lett. B **295** (1992) 269.
- [22] G. Parisi, Phys. Lett. B **74** (1978) 65;  
J.F. Donoghue, F.E. Low and S.Y. Pi, Phys. Rev. D **20** (1979) 2759.
- [23] S. Catani, Y.L. Dokshitzer, M. Olsson, G. Turnock and B.R. Webber, Phys. Lett. B **269** (1991) 432;  
N. Brown and W.J. Stirling, Phys. Lett. B **252** (1990) 657; Z. Phys. C **53** (1992) 629;  
W.J. Stirling *et al.*, Proceedings of the Durham Workshop, J. Phys. **G17** (1991) 1567;  
S. Bethke, Z. Kunszt, D.E. Soper and W.J. Stirling, Nucl. Phys. B **370** (1992) 310  
[Erratum-ibid. B **523** (1998) 681].
- [24] L.J. Dixon and A. Signer, Phys. Rev. Lett. **78** (1997) 811 [hep-ph/9609460]; Phys. Rev. D **56** (1997) 4031 [hep-ph/9706285].
- [25] J.J. van der Bij and E.W.N. Glover, Nucl. Phys. B **313** (1989) 237.
- [26] E. Maina, S. Moretti and D.A. Ross, JHEP **0304** (2003) 056 [hep-ph/0210015].
- [27] S. Moch, P. Uwer and S. Weinzierl, Phys. Rev. D **66** (2002) 114001 [hep-ph/0207043].
- [28] E.W.N. Glover, Nucl. Phys. Proc. Suppl. **116** (2003) 3 [arXiv:hep-ph/0211412].
- [29] F.V. Tkachov, Phys. Lett. B **100** (1981) 65;  
K.G. Chetyrkin and F.V. Tkachov, Nucl. Phys. B **B92** (1981) 159.
- [30] T. Gehrmann and E. Remiddi, Nucl. Phys. B **580** (2000) 485 [hep-ph/9912329].
- [31] S. Laporta, Int. J. Mod. Phys. A **15** (2000) 5087 [hep-ph/0102033].
- [32] T. Gehrmann and E. Remiddi, Nucl. Phys. B **601** (2001) 248 [hep-ph/0008287]; **601** (2001) 287 [hep-ph/0101124].
- [33] E. Remiddi and J.A.M. Vermaseren, Int. J. Mod. Phys. A **15** (2000) 725 [hep-ph/9905237];  
T. Gehrmann and E. Remiddi, Comput. Phys. Commun. **141** (2001) 296 [hep-ph/0107173];  
Comput. Phys. Commun. **144** (2002) 200 [hep-ph/0111255];  
D. Maître, Comput. Phys. Commun. **174** (2006) 222 [hep-ph/0507152].
- [34] Z. Nagy and Z. Trocsanyi, Phys. Rev. Lett. **79** (1997) 3604 [hep-ph/9707309];  
S. Weinzierl and D.A. Kosower, Phys. Rev. D **60** (1999) 054028 [hep-ph/9901277];
- [35] J. Campbell, M.A. Cullen and E.W.N. Glover, Eur. Phys. J. C **9** (1999) 245 [hep-ph/9809429].
- [36] S. Catani, Phys. Lett. B **427** (1998) 161 [hep-ph/9802439];  
G. Sterman and M.E. Tejeda-Yeomans, Phys. Lett. B **552** (2003) 48 [hep-ph/0210130].
- [37] A. Gehrmann-De Ridder and E.W.N. Glover, Nucl. Phys. B **517** (1998) 269 [hep-ph/9707224];  
J. Campbell and E.W.N. Glover, Nucl. Phys. B **527** (1998) 264 [hep-ph/9710255];  
F.A. Berends and W.T. Giele, Nucl. Phys. B **313** (1989) 595;  
V. Del Duca, A. Frizzo and F. Maltoni, Nucl. Phys. B **568** (2000) 211 [hep-ph/9909464];  
S. Catani and M. Grazzini, Phys. Lett. B **446** (1999) 143 [hep-ph/9810389]; Nucl. Phys. B **570** (2000) 287 [hep-ph/9908523].

- [38] Z. Bern, L.J. Dixon, D.C. Dunbar and D.A. Kosower, Nucl. Phys. B **425** (1994) 217 [hep-ph/9403226];  
D.A. Kosower, Nucl. Phys. B **552** (1999) 319 [hep-ph/9901201];  
D.A. Kosower and P. Uwer, Nucl. Phys. B **563** (1999) 477 [hep-ph/9903515];  
Z. Bern, V. Del Duca and C.R. Schmidt, Phys. Lett. B **445** (1998) 168 [hep-ph/9810409];  
Z. Bern, V. Del Duca, W.B. Kilgore and C.R. Schmidt, Phys. Rev. D **60** (1999) 116001 [hep-ph/9903516];  
S. Catani and M. Grazzini, Nucl. Phys. B **591** (2000) 435 [hep-ph/0007142].
- [39] Z. Kunszt and D.E. Soper, Phys. Rev. D **46** (1992) 192;  
S. Frixione, Z. Kunszt and A. Signer, Nucl. Phys. B **467** (1996) 399 [hep-ph/9512328];  
S. Catani and M.H. Seymour, Nucl. Phys. B **485** (1997) 291 [hep-ph/9605323];  
Z. Nagy and Z. Trocsanyi, Nucl. Phys. B **486** (1997) 189 [hep-ph/9610498].
- [40] D.A. Kosower, Phys. Rev. D **57** (1998) 5410 [hep-ph/9710213]; Phys. Rev. D **71** (2005) 045016 [hep-ph/0311272];  
A. Daleo, T. Gehrmann and D. Maître, JHEP **0704** (2007) 016 [hep-ph/0612257].
- [41] S. Catani and M. Grazzini, Phys. Rev. Lett. **98** (2007) 222002 [hep-ph/0703012].
- [42] A. Gehrmann-De Ridder, T. Gehrmann and E.W.N. Glover, Nucl. Phys. B **691** (2004) 195 [hep-ph/0403057].
- [43] D.A. Kosower, Phys. Rev. D **67** (2003) 116003 [hep-ph/0212097].
- [44] C. Anastasiou and K. Melnikov, Nucl. Phys. B **646** (2002) 220 [hep-ph/0207004];  
C. Anastasiou, L. J. Dixon, K. Melnikov and F. Petriello, Phys. Rev. D **69** (2004) 094008 [hep-ph/0312266].
- [45] A. Gehrmann-De Ridder, T. Gehrmann and G. Heinrich, Nucl. Phys. B **682** (2004) 265 [hep-ph/0311276].
- [46] A. Gehrmann-De Ridder, T. Gehrmann, E. W. N. Glover and G. Heinrich, Phys. Rev. Lett. **99** (2007) 132002 [arXiv:0707.1285 [hep-ph]].
- [47] S. Bethke, Prog. Part. Nucl. Phys. **58** (2007) 351 [hep-ex/0606035].
- [48] R.W.L. Jones, M. Ford, G.P. Salam, H. Stenzel and D. Wicke, JHEP **0312** (2003) 007.
- [49] S. Catani, G. Turnock and B. R. Webber, Phys. Lett. B **272** (1991) 368;  
E. Gardi and J. Rathsmann, Nucl. Phys. B **638** (2002) 243 [hep-ph/0201019].
- [50] S. Catani and B. R. Webber, Phys. Lett. B **427** (1998) 377 [hep-ph/9801350];  
E. Gardi and L. Magnea, JHEP **0308** (2003) 030 [hep-ph/0306094].
- [51] S. Catani and B. R. Webber, JHEP **9710** (1997) 005 [hep-ph/9710333].
- [52] A. Banfi, G. P. Salam and G. Zanderighi, JHEP **0201** (2002) 018 [hep-ph/0112156].
- [53] G. Dissertori, A. Gehrmann-De Ridder, T. Gehrmann, E.W.N. Glover, G. Heinrich and H. Stenzel, arXiv:0712.0327 [hep-ph].
- [A] T. Becher and M.D. Schwartz, JHEP **0807** (2008) 034 [0803.0342].
- [B] S. Weinzierl, Phys. Rev. Lett. **101** (2008) 162001 [0807.3241].